Substrate-Assisted Mechanism for the Degradation of *N*-Glycans by a Gut Bacterial Mannoside Phosphorylase

Mercedes Alfonso-Prieto,[▽] Irene Cuxart,[▽] Gabrielle Potocki-Véronèse, Isabelle André,* and Carme Rovira*

ABSTRACT: The unknown human gut bacterium mannoside phosphorylase (UhgbMP) is involved in the metabolization of eukaryotic *N*-glycans lining the intestinal epithelium, a factor associated with the onset and symptoms of inflammatory bowel diseases. In contrast with most glycoside phosphorylases, the putative catalytic acid of UhgbMP, Asp104, is far from the scissile glycosidic bond, challenging the classical Koshland mechanism. Using quantum mechanics/molecular mechanics metadynamics, we demonstrate that the enzyme operates by substrate-assisted catalysis via the 3-hydroxyl group of the mannosyl unit, following a $^{1}S_{5}/B_{2,5} \rightarrow [B_{2,5}]^{\ddagger} \rightarrow {}^{0}S_{2}$ conformational itinerary. Given the conservation of the active site hydrogen bond network across the family, this mechanism is expected to apply to other GH130 enzymes, as well as recently characterized mannoside phosphorylases with similar folds. Gaining insight into the catalytic reaction of these enzymes can aid the design of specific inhibitors to control interactions between gut microbes and the host.

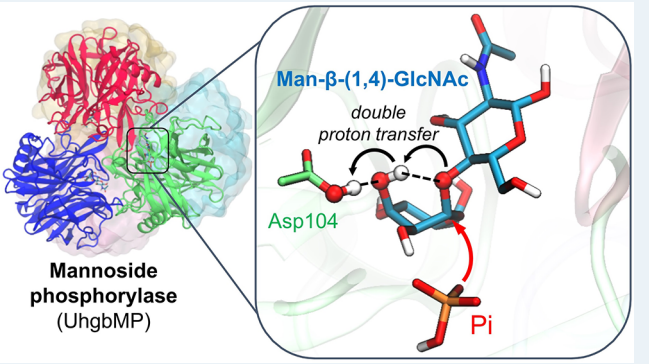

KEYWORDS: *N-glycans, microbiota, enzyme catalysis, catalytic reaction mechanism, glycoside phosphorylase, mannosides, quantum mechanics/molecular mechanics, metadynamics*

Enzymes produced by the gut microbiota play a major role in human health and disease.[1,2] In particular, gut bacterial glycolytic enzymes are responsible for the breakdown and metabolization of the complex carbohydrates of dietary,[3,4] microbial,[5,6] and human[7,8] origins. In addition, the over-prevalence of genes encoding gut bacterial enzymes involved in host glycan degradation and/or alteration of the mucosal gut microbiota structure is correlated to several diseases, such as inflammatory bowel diseases (IBDs).[9−11]

The unknown human gut bacterium mannoside phosphorylase (UhgbMP) was discovered by functional metagenomics and is produced by a so far unidentified intestinal bacterium of the *Bacteroides* genus.[12] This enzyme is essential to metabolize eukaryotic *N*-glycans contained in the gut, such as those of the mucus that lines the intestinal epithelium and those of the opportunistic pathogenic yeast *Candida albicans*.[6]

UhgbMP uses inorganic phosphate (Pi) to cleave the β-1,4 glycosidic bond between the nonreducing β-mannosyl residue and the neighboring *N*-acetyl-glucosamine in the eukaryotic *N*-glycan motif Man-β-(1,4)-chitobiose, releasing α-mannose-1-phosphate and chitobiose as follows:[12]

$$\text{Man-}\beta\text{-(1, 4)-(GlcNAc)}_2 + \text{Pi} \rightleftarrows \alpha\text{-Man-1-P} + \text{(GlcNAc)}_2 \quad (1)$$

The catalytic properties of UhgbMP have sparked great interest for both biomedical and biosynthetic applications. On one hand, UhgbMP and its homologues are potential therapeutic targets, as they are encoded by highly prevalent and abundant genes in the microbiomes of patients suffering from inflammatory bowel diseases.[12] On the other hand, UhgbMP can catalyze the *in vitro* synthesis of *N*-glycan core oligosaccharides very efficiently by reverse phosphorolysis[13,14] and thus may be used as a biosynthetic tool to produce these high-added-value products, which are very difficult and expensive to synthesize by other means.[12]

In contrast to some other members of the GH130 family, UhgbMP is a highly promiscuous enzyme, able to act on a large diversity of β-1,4-linked mannosides. It can act both on plant mannans and on long manno-oligosaccharides, allowing the production of *N*-glycan core motifs (β-1,4-mannosyl-chitobiose and β-1,4-mannosyl-*N*-acetyl-glucosamine) directly

Received: January 30, 2023

from plant mannan, inorganic phosphate, and chitobiose or *N*-acetylglucosamine.[12]

The design of UhgbMP inhibitors, as well as the utilization of UhgbMP and more generally that of mannoside phosphorylases as biosynthetic tools, requires further insight into their substrate recognition and catalytic mechanism. UhgbMP belongs to the glycoside hydrolase family 130 (GH130), which contains both mannosidases and phosphorylases that cleave β-mannosides at the nonreducing ends of their substrates.[15,16] UhgbMP is a homohexamer, with each monomer consisting of a five-bladed-propeller fold (Figure 1A), with the catalytic center located in the central cleft.

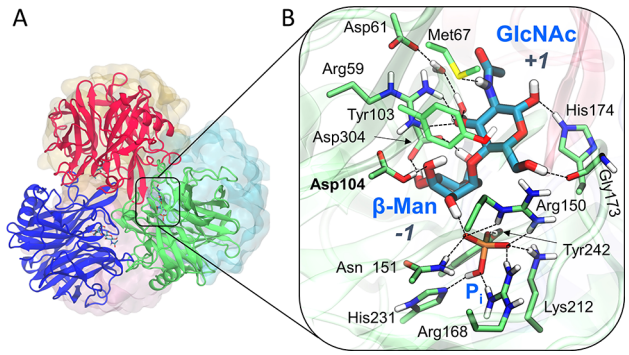

Figure 1. (A) Michaelis complex of the unknown human gut bacterium mannoside phosphorylase (UhgbMP), reconstructed from two crystal structures of UhgbMP complexes (PDB 4UDK and 4UDJ), after classical (force field-based) and QM/MM molecular dynamics (MD) simulations. Each protein subunit of hexameric UhgbMP is shown in a different color. The three front subunits are shown in cartoon representation, whereas the ones at the back are shown in surface representation. The substrate (Man-β-(1,4)-GlcNAc) and inorganic phosphate (Pi) are shown in licorice (only the ligands bound to the front three subunits are shown). (B) Detailed view of the enzyme active site. Only the polar hydrogens are shown for clarity.

Structural analyses have shown that the active site can accommodate a phosphate ion (Pi), mannose, and *N*-acetylglucosamine in the central furrow (Figure 1B).[17]

The catalytic mechanism of UhgbMP was initially assumed to be the general one for inverting GPs.[12,14,18] Inorganic phosphate acts as a nucleophile, attacking the anomeric carbon of the mannosyl ring at the -1 enzyme subsite (Figure 2A). The reaction is assisted by leaving group protonation by an acidic residue. Based on mutagenesis data and amino acid conservation analysis,[12] the putative catalytic acid of UhgbMP was identified as Asp104. However, the crystal structures of UhgbMP complexes[17] showed that the putative acid–base residue is not close to the glycosidic oxygen (Figures 1B and S1), unlike other GPs. Instead, Asp104 interacts with the 3-hydroxyl group of the donor sugar, which in turn might interact with the glycosidic oxygen (Figure 1B).

The unusual position of the catalytic acid in UhgbMP led to the proposal of a novel mechanism, originally put forward for β-1,4-mannosylglucose phosphorylase (MGP),[19] in which Asp104 transfers a proton to the glycosidic oxygen through the 3-OH group of the mannosyl unit (*i.e.*, the proton relay illustrated in Figure 2B).[17,19] Interestingly, the particular disposition of the catalytic acid and the sugar 3-OH in UhgbMP has also been observed for other GPs of the GH130 family for which structural information is available (Tables S1 and S2).[16,19−22] Recently, it was been found in a dual-activity glycosyltransferase-phosphorylase of family GT108, which shares the fold with GH130 β-mannoside phosphorylases.[23] This novel mechanistic proposal, in particular the elusive transition state configuration, has not been assessed by computational approaches yet.

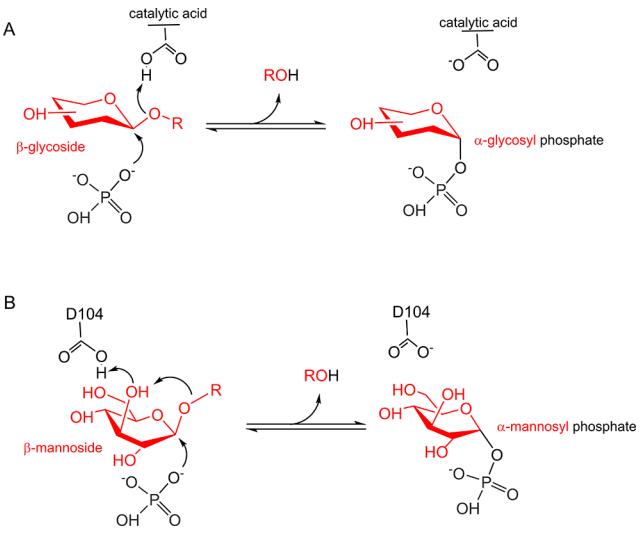

Figure 2. (A) General mechanism of inverting glycoside phosphorylases. (B) Substrate-assisted reaction proposed for GH130 mannoside phosphorylases.

In the light of crystallographic structures of UhgbMP,[17] we modeled its catalytic reaction mechanism using molecular dynamics (MD) and quantum mechanics/molecular mechanics (QM/MM) methods based on density functional theory (DFT). Our simulations show that the phosphorolysis reaction indeed follows a substrate-assisted mechanism involving proton relay via the 3-hydroxyl group of the mannosyl ring, which nevertheless adopts the classical boat ($B_{2,5}$) transition state conformation observed in most β-mannosidases.[24,25] Moreover, we demonstrate that the complete hexameric organization of the enzyme is required for substrate recognition and identify critical enzyme amino acid residues responsible for substrate specificity.

The X-ray structures of UhgbMP in complex with inorganic phosphate (Pi), β-mannose, and *N*-acetylglucosamine (PDB code 4UDK),[17] as well as that of the enzyme complex with Pi and mannose (PDB code 4UDJ),[17] were used to build the Michaelis complex, *i.e.*, UhgbMP in complex with Pi and Man-β-(1,4)-GlcNAc (see SI section 1 and Figure S1). Using NAMD,[26] molecular dynamics (MD) simulations were performed for three different oligomeric forms of the enzyme: monomer, dimer, and hexamer (see SI sections 2 and 3). The simulations for the hexameric form show that the substrate is stably bound throughout the entire simulations (Figures 1 and S1–S3). Here, the GlcNAc sugar at the *+1* subsite is strongly engaged in stabilizing interactions with residues of the same protein subunit (most notably Arg59, Tyr103, and His174; Figure 1B). In contrast, the simulations for the monomeric and dimeric forms of the enzyme show that the GlcNAc sugar at the *+1* subsite is quite flexible and solvent-exposed (Figures S8a and b and S9), favoring the displacement of the substrate by water molecules and the occurrence of hydrolysis (*i.e.*, glycosidic bond cleavage with a water molecule) instead of phosphorolysis (*i.e.*, the analogous reaction with phosphate).

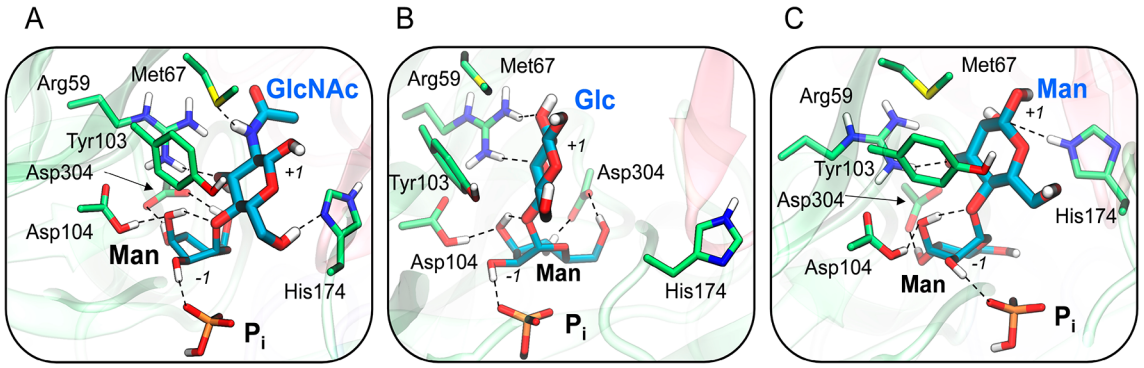

Figure 3. Main enzyme−sugar interactions for different substrates bound to the promiscuous UhgMP enzyme: (A) Man-β-(1,4)-GlcNAc, (B) Man-β-(1,4)-Glc, and (C) Man-β-(1,4)-Man.

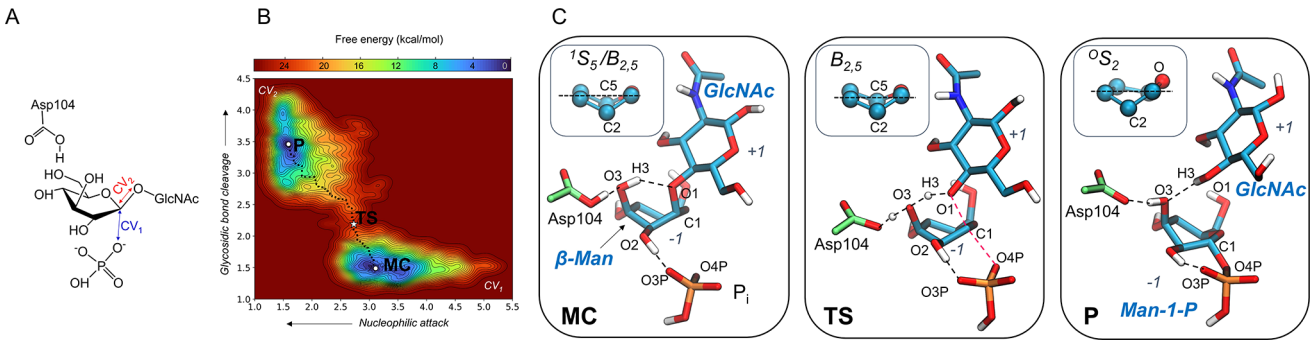

Figure 4. (A) Collective variables used in the QM/MM metadynamics simulations. (B) Free-energy surface of the phosphorolysis reaction catalyzed by UhgbMP. Contour lines are shown at 1 kcal/mol. (C) Relevant states along the reaction coordinate. Only the polar hydrogens are displayed for the sake of clarity. Relevant hydrogen bonds are shown as black dashed lines. Bonds being formed or broken at the TS are represented by the red dashed line. The insets show the ring conformations of the mannose sugar at the -1 subsite; labels indicate the atoms out of the pyranose ring plane.

The distances relevant for the phosphorolysis reaction show larger fluctuations in the monomer and dimer simulations (Figure S10) than in the hexamer counterpart (Figure S3), indicating the increased sampling of noncatalytically competent configurations for the low-order oligomers. Therefore, our simulations show that the hexameric organization of UhgbMP is needed to form a stable, catalytically competent Michaelis complex for the phosphorolysis reaction. This is consistent with the hexamer being the only oligomeric state captured by X-ray structural and SAXS analyses, as well as by size-exclusion chromatography multiangle laser light scattering experiments.[17]

Additional MD simulations for the hexameric enzyme were performed considering other substrates differing in the type of sugar acceptor occupying the *+1* subsite (*i.e.*, Man-Man or Man-Glc rather than Man-GlcNAc); see SI section 4. Our results show that the sugar at the *+1* subsite is able to establish persistent hydrogen bond interactions with Arg59, as well as CH−π interactions with Tyr103 (Figures 3 and S11−S13) in all cases. This suggests that Arg59 and Tyr103 are critical for substrate recognition and could play a role in the known promiscuity of UhgbMP with respect to β-1,4-linked mannosides. Two additional residues, Met67 and His174, were found to interact in different ways with the substrates (Figures 3 and S11−S13) and could thus relate to differences observed in their K_m values.

Interestingly, the mannosyl ring in the -1 subsite adopts a distorted $^1S_5/B_{2,5}$ conformation (Figures 1B and S2c). This conformation, typically observed in β-mannosidases,[25] places the leaving group in an axial orientation, facilitating its departure during the S_N2 reaction and, at the same time, alleviates the steric hindrance of the axial 2-OH during the nucleophilic attack. The $^1S_5/B_{2,5}$ conformation of the mannosyl ring in UhgbMP is stabilized by the hydrogen bond between the 2-OH group and the Pi, as well as the bidentate hydrogen bond with Asp304 (involving the 4- and 5-OH mannose substituents) (Figure 1B). The important role of Asp304 in maintaining the reactive (*i.e.*, suitably distorted) conformation of the mannosyl ring explains why the Asp304Asn enzyme variant retains only 4% of the wild-type activity.[12]

Regarding intermolecular interactions involving the mannosyl ring at the -1 subsite, the MD simulations show that the putative catalytic acid (Asp104) forms a persistent hydrogen bond with the 3-OH, which in turn interacts with the glycosidic oxygen (Figures 1B and S3). Such a hydrogen bond network seems particularly suited for relaying protons. Nevertheless, the reaction coordinate cannot be ascertained based on the structure alone.

A priori, a proton transfer via 3-OH seems unlikely given the high pK_a of a sugar hydroxyl group (>13).[27] However, the hydrogen bond network $OH_{Asp104}\cdots O3-H\cdots O1$ is likely to increase the acidity of the O3−H group. In fact, there are enzymes in which hydroxyl groups play a role in catalysis,[28−30] including an endomannosidase from family GH99 in which an epoxide intermediate involving the sugar O2 atom is formed.[31] In UhgbMP, the reaction via 3-OH requires Asp104 to be protonated. This is facilitated by the water-shielded active site and the proximity of the inorganic phosphate, which is

expected to raise the pK_a of Asp104. Indeed, pK_a estimations with the H++ web server[32] show this trend (Table S3). Similarly, in classical inverting GHs, the acid−base residue has a higher pK_a than a normal carboxylic acid due to the presence of the negatively charged catalytic base at 9−10 Å.[33−35] In addition, MD simulations performed with unprotonated Asp104 show that the hydrogen bond network needed for the reaction to take place is disrupted (see SI section 5 and Figure S14).[17] This suggests that Asp104 is protonated in the reactive complex.

To model the catalytic reaction, we selected one snapshot of the last part of the classical MD simulation of the enzyme complex with Man-β-(1,4)-GlcNAc and Pi and performed QM/MM MD simulations using the approach developed by Laio et al.,[36] as implemented in the CPMD code.[36,37] The full substrate, the putative catalytic residue Asp104, the Pi, and the His that interacts with its OH group (His231) were included in the QM region (77 atoms, Figure S15). DFT was used to describe the atoms of the QM region, along with the PBE functional and a plane wave basis set (70 Ry cutoff), whereas the atoms of the MM region (195513 atoms) were treated with the AMBER force field.[38] This approach has previously been used to model mechanisms in carbohydrate-active enzymes,[39−43] including the phosphorolysis reaction in an engineered GH.[44]

The chemical reaction was activated by QM/MM metadynamics using two collective variables (CVs) that describe the main covalent bonds that are formed/broken during the reaction. The first CV (Figure 4A) was taken as the distance between the anomeric carbon of the β-mannosyl and the closest oxygen atom of the incoming phosphate to drive the nucleophilic attack. The second CV was taken as the glycosidic bond distance to trigger its cleavage. The two collective variables involved neither Asp104 (the putative catalytic acid) nor the 3-OH group, thus the chosen CVs do not preselect any proton donor to the glycosidic oxygen or the proton transfer pathway.

The QM/MM metadynamics simulation successfully drove the reactants (UhgbMP in complex with Man-β-1,4-GlcNAc and Pi) toward products (the enzyme complex with α-Man-1-P and GlcNAc). The reconstructed free energy surface (FES) (Figure 4B) shows only two minima, corresponding to the reactants (the Michaelis complex, MC) and the products (P), that are separated by a single transition state (TS). The location of the TS in the free-energy surface was further assessed by committor analysis (Figure S17). The shape of the FES indicates that the phosphorolysis reaction of UhgbMP proceeds in one single concerted S_N2 reaction, as expected for an inverting GP.[14,18] The computed free-energy barrier amounts to 21.6 kcal/mol, in good agreement with the value estimated from the experimentally measured reaction rate for a similar substrate (19.8 kcal/mol for the phosphorolysis of Man-β-(1,4)-$(GlcNAc)_2$, applying transition-state theory at the experimental temperature of 310 K).[12]

Representative structures of the most relevant states along the reaction pathway (MC, TS, and P) are shown in Figure 4C. The MC state features a distorted β-mannosyl ring ($^1S_5/B_{2,5}$). The boat conformation places the leaving group in an axial orientation, lengthening the glycosidic bond distance (1.50 Å) compared to an isolated mannose (1.40 Å),[45] which preactivates the substrate for catalysis. In addition, the 2-OH group of the mannosyl ring forms a hydrogen bond with the Pi, keeping it close to the anomeric carbon in an optimal configuration for nucleophilic attack (C1···O_{4P} = 3.41 Å; Table 1). The reaction begins with the elongation of the glycosidic bond (C1−O1) as the Pi approaches the sugar anomeric carbon. Simultaneously, the O3−H distance increases as Asp104 tightens its hydrogen bond with O3. At the reaction TS (Figure 3C), the proton of Asp104 is transferred to O3, with the latter in turn delivering its proton to the glycosidic oxygen (O1). The glycosidic bond is being broken (C1−O1 = 2.19 Å) while the O_{4P} atom is still far from the anomeric carbon (C1−O_{4P} = 2.57 Å), indicating a dissociative TS (Figure 4C). Similar nucleophilic distances have been observed for the phosphorolysis reaction in a GH using the same QM/MM approach.[44] The $B_{2,5}$ conformation of the β-mannosyl ring at the TS, with an almost coplanar configuration of the C5−O−C1−C2 atoms, evidences the formation of an oxocarbenium ion-like species. The interaction between the 2-OH and the O_{3P} atom of the Pi (stronger in the TS compared to the MC, see Table 1) also contributes to TS stabilization by the inductive effect on the anomeric carbon.[46,47] It has been shown that interactions via the 2-OH stabilize the TS by about 10 kcal/mol in glycosidases.[47,48] Finally, the Pi binds to the mannosyl anomeric carbon, forming the Man-1-P product (with $^0S_2$ conformation) and releasing GlcNAc (Figure 4C). Therefore, the QM/MM metadynamics simulations reveal that, unlike classical inverting GHs and GPs,[39,49] UhgbMP operates by substrate-assisted catalysis involving a concerted double proton transfer via the 3-OH. Moreover, the mannosyl ring still follows the $^1S_5/B_{2,5} \rightarrow [B_{2,5}]^{\ddagger} \rightarrow {}^0S_2$ conformational itinerary, as also found in other β-mannosidases.[25]

Table 1. Main Reaction Distances (in Å) at Relevant States along the Reaction Coordinate

distance	MC	TS[a]	P
C1−O_{4P}	3.41 ± 0.51	2.57	181 ± 0.42
C1−O1	1.50 ± 0.09	2.19	3.51 ± 0.44
C1−O5	1.41 ± 0.04	1.28	1.36 ± 0.06
O3−H_{Asp104}	1.48 ± 0.13	1.22	1.04 ± 0.03
O3−H3	1.01 ± 0.04	1.21	1.95 ± 0.19
H3−O1	1.79 ± 0.15	1.27	1.00 ± 0.03
H2−O_{3P}	1.73 ± 0.31	1.50	1.73 ± 0.19

[a]Obtained from committor analysis over the FES.

As mentioned above, the chosen CVs do not bias the proton transfer pathway. Therefore, the fact that the double proton transfer occurs seamlessly upon glycosidic bond cleavage clearly indicates that the system prefers to protonate the leaving group through the 3-OH of the mannosyl ring rather than though direct proton transfer from Asp104 to O1. Most likely, the two hydrogen bonds (OH_{Asp104}···O3−H···O1) provide the geometric restraints and the energetic stabilization needed for the simultaneous two-proton transfer. The hydrogen bond network between the catalytic Asp and the substrate allows the reaction to proceed (see the Supporting Movie) with the least nuclear motion and the least activation energy,[50,51] in contrast to the large reorganization of the active site needed for Asp104 to approach the glycosidic oxygen to transfer the proton directly. In this regard, the active site architecture of UhgbMP constitutes another example of a hydrogen-bonded network for synchronous multiproton transfers, as employed in a wide diversity of enzymes.[52−54]

Interestingly, the hydrogen bond network involved in the concerted double proton transfer is conserved across GH130

enzymes (Tables S1 and S2) and thus the substrate-assisted mechanism described here for UhgbMP may also apply to other GH130 enzymes such as MGP,[19] β-1,4-mannooligosaccharide phosphorylase (RaMP2),[21] and β-1,2-mannobiose phosphorylase (Lin0857).[20] Interestingly, it was recently found that some glycosyltransferases from the GT108 family are mannose phosphorylases (MPs) that share a fold and activity with GH130 MPs, including a similarly positioned catalytic acid.[23] Our study predicts that all these MPs will feature a substrate-assisted catalytic mechanism similar to the one that we have characterized herein.

In conclusion, our classical (force field-based) MD and QM/MM metadynamics simulations on UhgbMP have unveiled the mechanism of a GH130 mannoside phosphorylase for which the catalytic acid is not in the "canonical" position (Figure 2A). We demonstrate that UhgbMP uses a substrate-assisted mechanism in which the 3-hydroxyl group of the mannosyl unit acts as a proton relay between Asp104 and the glycosidic oxygen atom (Figure 2B), solving this intriguing mechanistic question. We provide the precise itinerary of the substrate during catalysis, which can serve in the design of not only more efficient enzymes as biosynthetic tools but also ligands able to inhibit *N*-glycan degradation by GH130 enzymes. The mechanism disclosed herein is expected to apply to other GH130 enzymes with phosphorolytic activity,[15] as well as the recently reported dual-activity GT108 mannoside phosphorylases.[23]

■ ASSOCIATED CONTENT

Supporting Information

The Supporting Information is available free of charge at https://pubs.acs.org/doi/10.1021/acscatal.3c00451.

Trajectory of the metadynamics simulation corresponding to the reactive event (MP4)

System preparation, oligomerization state and substrate promiscuity of UhgbMP, investigation of the protonation state of Asp104, computational details, and the Supporting Movie caption (PDF)

■ AUTHOR INFORMATION

Corresponding Authors

Isabelle André − *Toulouse Biotechnology Institute (TBI), Université de Toulouse, CNRS, INRAE, INSA, F-31077 Toulouse, France;* orcid.org/0000-0001-6280-4109; Email: isabelle.andre@insa-toulouse.fr

Carme Rovira − *Departament de Química Inorgànica i Orgànica, Universitat de Barcelona, 08028 Barcelona, Spain; Institució Catalana de Recerca i Estudis Avançats (ICREA), 08010 Barcelona, Spain;* orcid.org/0000-0003-1477-5010; Email: c.rovira@ub.edu

Authors

Mercedes Alfonso-Prieto − *Departament de Química Inorgànica i Orgànica, Universitat de Barcelona, 08028 Barcelona, Spain;* Present Address: Institute for Advanced Simulations IAS-5 and Institute of Neuroscience and Medicine INM-9, Computational Biomedicine, Forschungszentrum Jülich, Jülich 52425, Germany; orcid.org/0000-0003-4509-4517

Irene Cuxart − *Departament de Química Inorgànica i Orgànica, Universitat de Barcelona, 08028 Barcelona, Spain;* orcid.org/0000-0002-8413-9725

Gabrielle Potocki-Véronèse − *Toulouse Biotechnology Institute (TBI), Université de Toulouse, CNRS, INRAE, INSA, F-31077 Toulouse, France*

Complete contact information is available at: https://pubs.acs.org/10.1021/acscatal.3c00451

Author Contributions

[▽]M.A-P and I.C. contributed equally.

Notes

The authors declare no competing financial interest.

■ ACKNOWLEDGMENTS

C.R. thanks the Spanish Ministry of Science, Innovation and Universities (MICINN/AEI/FEDER, UE, PID2020-118893GB-100), the Spanish Structures of Excellence María de Maeztu (CEX2021-001202-M) and the Agency for Management of University and Research Grants of Generalitat de Catalunya (AGAUR, AGAUR, 2021-SGR-00680). I.A. and G.P.-V. thank the French National Research Agency (ANR project OLIGOMET, ANR-16-CE20-0006-03) and the European Union's Horizon 2020 framework program (Grant FNR-2020-SEP-210639118, RadicalZ). The authors are thankful for the technical support provided by the Barcelona Supercomputing Center (BSC) and Red Nacional de Supercomputación (RES) for computer resources at MareNostrum IV and CTE-Power supercomputers (application project QH-2022-3-0002). We are also grateful for the computer time provided on the TGCC-Curie supercomputer under the allocations t201608765 and A0030807565 and the Computing Mesocenter of Région Midi-Pyrénées (CALMIP, Toulouse, France) under allocation 16004. I.C. acknowledges a predoctoral fellowship from MICINN (ref. PRE2019-089272). M.A.-P. acknowledges financial support from the Government of Catalonia (Commissioner for Universities and Research; Department of Innovation, Universities and Enterprise) and the European Union through a Beatriu de Pinós fellowship (BP-B 2013).

■ REFERENCES

(1) Kau, A. L.; Ahern, P. P.; Griffin, N. W.; Goodman, A. L.; Gordon, J. I. Human Nutrition, the Gut Microbiome and the Immune System. *Nature* **2011**, *474*, 327−336.

(2) Wardman, J. F.; Bains, R. K.; Rahfeld, P.; Withers, S. G. Carbohydrate-active enzymes (CAZymes) in the gut microbiome. *Nat. Rev. Microbiol.* **2022**, *20*, 542−556.

(3) Tasse, L.; Bercovici, J.; Pizzut-Serin, S.; Robe, P.; Tap, J.; Klopp, C.; Cantarel, B. L.; Coutinho, P. M.; Henrissat, B.; Leclerc, M.; Doré, J.; Monsan, P.; Remaud-Simeon, M.; Potocki-Veronese, G. Functional metagenomics to mine the human gut microbiome for dietary fiber catabolic enzymes. *Genome Res.* **2010**, *20*, 1605−1612.

(4) El Kaoutari, A.; Armougom, F.; Gordon, J. I.; Raoult, D.; Henrissat, B. The Abundance and Variety of Carbohydrate-Active Enzymes in the Human Gut Microbiota. *Nat. Rev. Microbiol.* **2013**, *11*, 497−504.

(5) Cuskin, F.; Lowe, E. C.; Temple, M. J.; Zhu, Y.; Cameron, E. A.; Pudlo, N. A.; Porter, N. T.; Urs, K.; Thompson, A. J.; Cartmell, A.; Rogowski, A.; Hamilton, B. S.; Chen, R.; Tolbert, T. J.; Piens, K.; Bracke, D.; Vervecken, W.; Hakki, Z.; Speciale, G.; Munoz-Munoz, J. L.; Day, A.; Pena, M. J.; McLean, R.; Suits, M. D.; Boraston, A. B.; Atherly, T.; Ziemer, C. J.; Williams, S. J.; Davies, G. J.; Abbott, D. W.; Martens, E. C.; Gilbert, H. J. Human gut *Bacteroidetes* can utilize yeast mannan through a selfish mechanism. *Nature* **2015**, *517*, 165−169.

(6) Li, A.; Laville, E.; Tarquis, L.; Lombard, V.; Ropartz, D.; Terrapon, N.; Henrissat, B.; Guieysse, D.; Esque, J.; Durand, J.;

Morgavi, D. P.; Potocki-Veronese, G. Analysis of the diversity of the glycoside hydrolase family 130 in mammal gut microbiomes reveals a novel mannoside-phosphorylase function. *Microb. Genom.* **2020**, *6*, mgen000404.
(7) Wada, J.; Ando, T.; Kiyohara, M.; Ashida, H.; Kitaoka, M.; Yamaguchi, M.; Kumagai, H.; Katayama, T.; Yamamoto, K. *Bifidobacterium bifidum* Lacto-N-Biosidase, a Critical Enzyme for the Degradation of Human Milk Oligosaccharides with a Type 1 Structure. *AEM* **2008**, *74*, 3996−4004.
(8) Crouch, L. I.; Liberato, M. V.; Urbanowicz, P. A.; Baslé, A.; Lamb, C. A.; Stewart, C. J.; Cooke, K.; Doona, M.; Needham, S.; Brady, R. R.; Berrington, J. E.; Madunic, K.; Wuhrer, M.; Chater, P.; Pearson, J. P.; Glowacki, R.; Martens, E. C.; Zhang, F.; Linhardt, R. J.; Spencer, D. I. R.; Bolam, D. N. Prominent members of the human gut microbiota express endo-acting O-glycanases to initiate mucin breakdown. *Nat. Commun.* **2020**, *11*, 4017.
(9) Huttenhower, C.; Kostic, A. D.; Xavier, R. J. Inflammatory Bowel Disease as a Model for Translating the Microbiome. *Immunity* **2014**, *40*, 843−854.
(10) Sheng, Y. H.; Hasnain, S. Z.; Florin, T. H.; McGuckin, M. A. Mucins in Inflammatory Bowel Diseases and Colorectal Cancer. *J. Gastroenterol. Hepatol.* **2012**, *27*, 28−38.
(11) Tauzin, A. S.; Pereira, M. R.; Van Vliet, L. D.; Colin, P. Y.; Laville, E.; Esque, J.; Laguerre, S.; Henrissat, B.; Terrapon, N.; Lombard, V.; Leclerc, M.; Doré, J.; Hollfelder, F.; Potocki-Veronese, G. Investigating host-microbiome interactions by droplet based microfluidics. *Microbiome* **2020**, *8*, 141.
(12) Ladeveze, S.; Tarquis, L.; Cecchini, D. A.; Bercovici, J.; Andre, I.; Topham, C. M.; Morel, S.; Laville, E.; Monsan, P.; Lombard, V.; Henrissat, B.; Potocki-Veronese, G. Role of glycoside phosphorylases in mannose foraging by human gut bacteria. *J. Biol. Chem.* **2013**, *288*, 32370−32383.
(13) Kitaoka, M. Diversity of phosphorylases in glycoside hydrolase families. *Appl. Microbiol. Biotechnol.* **2015**, *99*, 8377−8390.
(14) Puchart, V. Glycoside phosphorylases: structure, catalytic properties and biotechnological potential. *Biotechnol. Adv.* **2015**, *33*, 261−276.
(15) Li, A.; Benkoulouche, M.; Ladeveze, S.; Durand, J.; Cioci, G.; Laville, E.; Potocki-Veronese, G. Discovery and Biotechnological Exploitation of Glycoside-Phosphorylases. *Int. J. Mol. Sci.* **2022**, *23*, 3043.
(16) Cuskin, F.; Baslé, A.; Ladevèze, S.; Day, A. M.; Gilbert, H. J.; Davies, G. J.; Potocki-Véronèse, G.; Lowe, E. C. The GH130 family of mannoside phosphorylases contains glycoside hydrolases that target β-1,2 mannosidic linkages in *Candida* mannan. *J. Biol. Chem.* **2015**, *290*, 25023−25033.
(17) Ladeveze, S.; Cioci, G.; Roblin, P.; Mourey, L.; Tranier, S.; Potocki-Veronese, G. Structural Bases for N-glycan Processing by Mannoside Phosphorylase. *Acta Crystallogr. D Biol. Crystallogr.* **2015**, *71*, 1335−1346.
(18) Luley-Goedl, C.; Nidetzky, B. Carbohydrate synthesis by disaccharide phosphorylases: reactions, catalytic mechanisms and application in the glycosciences. *Biotechnol. J.* **2010**, *5*, 1324−1338.
(19) Nakae, S.; Ito, S.; Higa, M.; Senoura, T.; Wasaki, J.; Hijikata, A.; Shionyu, M.; Ito, S.; Shirai, T. Structure of Novel Enzyme in Mannan Biodegradation Process 4-O-β-D-Mannosyl-D-Glucose Phosphorylase MGP. *J. Mol. Biol.* **2013**, *425*, 4468−4478.
(20) Tsuda, T.; Nihira, T.; Chiku, K.; Suzuki, E.; Arakawa, T.; Nishimoto, M.; Kitaoka, M.; Nakai, H.; Fushinobu, S. Characterization and Crystal Structure Determination of β-1,2-Mannobiose Phosphorylase from *Listeria innocua*. *FEBS Lett.* **2015**, *589*, 3816−3821.
(21) Ye, Y.; Saburi, W.; Odaka, R.; Kato, K.; Sakurai, N.; Komoda, K.; Nishimoto, M.; Kitaoka, M.; Mori, H.; Yao, M. Structural Insights into the Difference in Substrate Recognition of Two Mannoside Phosphorylases from Two GH130 Subfamilies. *FEBS Lett.* **2016**, *590*, 828−837.
(22) Dai, L.; Chang, Z.; Yang, J.; Liu, W.; Yang, Y.; Chen, C. C.; Zhang, L.; Huang, J. W.; Sun, Y.; Guo, R. T. Structural investigation of a thermostable 1,2-β-mannobiose phosphorylase from *Thermoanaerobacter sp.* X-514. *Biochem. Biophys. Res. Commun.* **2021**, *579*, 54−61.
(23) Sernee, M. F.; Ralton, J. E.; Nero, T. L.; Sobala, L. F.; Kloehn, J.; Vieira-Lara, M. A.; Cobbold, S. A.; Stanton, L.; Pires, D. E. V.; Hanssen, E.; Males, A.; Ward, T.; Bastidas, L. M.; van der Peet, P. L.; Parker, M. W.; Ascher, D. B.; Williams, S. J.; Davies, G. J.; McConville, M. J. A Family of Dual-Activity Glycosyltransferase-Phosphorylases Mediates Mannogen Turnover and Virulence in *Leishmania* Parasites. *Cell Host Microbe* **2019**, *26*, 385−399.
(24) Davies, G. J.; Planas, A.; Rovira, C. Conformational analyses of the reaction coordinate of glycosidases. *Acc. Chem. Res.* **2012**, *45*, 308−316.
(25) Rovira, C.; Males, A.; Davies, G. J.; Williams, S. J. Mannosidase mechanism: at the intersection of conformation and catalysis. *Curr. Opin. Struct. Biol.* **2020**, *62*, 79−92.
(26) Phillips, J. C.; Braun, R.; Wang, W.; Gumbart, J.; Tajkhorshid, E.; Villa, E.; Chipot, C.; Skeel, R. D.; Kale, L.; Schulten, K. Scalable molecular dynamics with NAMD. *J. Comput. Chem.* **2005**, *26*, 1781−1802.
(27) Fasman, G. D. *Handbook of Biochemistry and Molecular Biology: Physical and Chemical Data*, 3d ed ed.; CRC Press: Boca Raton, FL, 1976.
(28) Schmeing, T. M.; Huang, K. S.; Kitchen, D. E.; Strobel, S. A.; Steitz, T. A. Structural insights into the roles of water and the 2' hydroxyl of the P site tRNA in the peptidyl transferase reaction. *Mol. Cell* **2005**, *20*, 437−448.
(29) Hoff, K. G.; Avalos, J. L.; Sens, K.; Wolberger, C. Insights into the sirtuin mechanism from ternary complexes containing NAD^+ and acetylated peptide. *Structure* **2006**, *14*, 1231−1240.
(30) Beringer, M.; Rodnina, M. V. The ribosomal peptidyl transferase. *Mol. Cell* **2007**, *26*, 311−321.
(31) Sobala, L. F.; Speciale, G.; Zhu, S.; Raich, L.; Sannikova, N.; Thompson, A. J.; Hakki, Z.; Lu, D.; Shamsi Kazem Abadi, S.; Lewis, A. R.; Rojas-Cervellera, V.; Bernardo-Seisdedos, G.; Zhang, Y.; Millet, O.; Jimenez-Barbero, J.; Bennet, A. J.; Sollogoub, M.; Rovira, C.; Davies, G. J.; Williams, S. J. An Epoxide Intermediate in Glycosidase Catalysis. *ACS Cent. Sci.* **2020**, *6*, 760−770.
(32) Anandakrishnan, R.; Aguilar, B.; Onufriev, A. V. H++ 3.0: automating pK prediction and the preparation of biomolecular structures for atomistic molecular modeling and simulations. *Nucleic Acids Res.* **2012**, *40*, W537−W541.
(33) McIntosh, L. P.; Hand, G.; Johnson, P. E.; Joshi, M. D.; Körner, M.; Plesniak, L. A.; Ziser, L.; Wakarchuk, W. W.; Withers, S. G. The pKa of the general acid/base carboxyl group of a glycosidase cycles during catalysis: a ^{13}C-NMR study of bacillus circulans xylanase. *Biochemistry* **1996**, *35*, 9958−9966.
(34) Anderson, D. E.; Lu, J.; McIntosh, L. P.; Dahlquist, F. W. The Folding, Stability and Dynamics of T4 Lysozyme: A Perspective Using Nuclear Magnetic Resonance. In *NMR of Proteins*; Clore, G. M., Gronenborn, A. M., Eds.; Red Globe Press: London, UK, 1993; pp 258−304.
(35) Harris, T. K.; Turner, G. J. Structural Basis of Perturbed pK_a Values of Catalytic Groups in Enzyme Active Sites. *IUBMB Life* **2002**, *53*, 85−98.
(36) Laio, A.; VandeVondele, J.; Rothlisberger, U. A Hamiltonian electrostatic coupling scheme for hybrid Car-Parrinello molecular dynamics simulations. *J. Chem. Phys.* **2002**, *116*, 6941−6947.
(37) *CPMD Program*, http://www.cpmd.org/, Copyright IBM Corp 1990−2003, Copyright MPI für Festkörperforschung Stuttgart 1997−2001.
(38) Case, D. A.; Darden, T. A.; Cheatham, T. E.; Simmerling, C.; Wang, J.; Duke, R.; Luo, R.; Crowley, M. F.; Walker, R.; Zhang, W.; Merz, K. M.; Wang, B.; Hayik, S.; Roitberg, A. E.; Seabra, G.; Kolossváry, I.; Wong, K. F.; Paesani, F.; Vanicek, J.; Wu, X.; Brozell, S.; Steinbrecher, T.; Gohlke, H.; Yang, L.; Tan, C.; Mongan, J.; Hornak, V.; Cui, G.; Mathews, D. H.; Seetin, M. G.; Sagui, C.; Babin, V.; Kollman, P. *AMBER 11*; University of California: San Francisco, CA, 2010.

(39) Coines, J.; Raich, L.; Rovira, C. Modeling catalytic reaction mechanisms in glycoside hydrolases. *Curr. Opin. Chem. Biol.* **2019**, *53*, 183−191.
(40) Ardèvol, A.; Rovira, C. Reaction mechanisms in carbohydrate-active enzymes: glycoside hydrolases and glycosyltransferases. Insights from ab initio quantum mechanics/molecular mechanics dynamic simulations. *J. Am. Chem. Soc.* **2015**, *137*, 7528−7547.
(41) Cuxart, I.; Coines, J.; Esquivias, O.; Faijes, M.; Planas, A.; Biarnes, X.; Rovira, C. Enzymatic Hydrolysis of Human Milk Oligosaccharides. The Molecular Mechanism of *Bifidobacterium Bifidum* Lacto-N-biosidase. *ACS Catal.* **2022**, *12*, 4737−4743.
(42) Bilyard, M. K.; Bailey, H. J.; Raich, L.; Gafitescu, M. A.; Machida, T.; Iglesias-Fernandez, J.; Lee, S. S.; Spicer, C. D.; Rovira, C.; Yue, W. W.; Davis, B. G. Palladium-mediated enzyme activation suggests multiphase initiation of glycogenesis. *Nature* **2018**, *563*, 235−240.
(43) Iglesias-Fernandez, J.; Hancock, S. M.; Lee, S. S.; Khan, M.; Kirkpatrick, J.; Oldham, N. J.; McAuley, K.; Fordham-Skelton, A.; Rovira, C.; Davis, B. G. A front-face 'S_Ni synthase' engineered from a retaining 'double-S_N2' hydrolase. *Nat. Chem. Biol.* **2017**, *13*, 874−881.
(44) Teze, D.; Coines, J.; Raich, L.; Kalichuk, V.; Solleux, C.; Tellier, C.; Andre-Miral, C.; Svensson, B.; Rovira, C. A Single Point Mutation Converts GH84 O-GlcNAc Hydrolases into Phosphorylases: Experimental and Theoretical Evidence. *J. Am. Chem. Soc.* **2020**, *142*, 2120−2124.
(45) Ardèvol, A.; Biarnés, X.; Planas, A.; Rovira, C. The conformational free-energy landscape of beta-D-mannopyranose: evidence for a $^{1}S_5 \rightarrow B_{2,5} \rightarrow {}^{O}S_2$ catalytic itinerary in beta-mannosidases. *J. Am. Chem. Soc.* **2010**, *132*, 16058−16065.
(46) White, A.; Tull, D.; Johns, K.; Withers, S. G.; Rose, D. R. Crystallographic observation of a covalent catalytic intermediate in a β-glycosidase. *Nat. Struct. Biol.* **1996**, *3*, 149−154.
(47) Namchuk, M. N.; Withers, S. G. Mechanism of *Agrobacterium* β-glucosidase: kinetic analysis of the role of noncovalent enzyme/substrate interactions. *Biochemistry* **1995**, *34*, 16194−16202.
(48) Raich, L.; Borodkin, V.; Fang, W.; Castro-Lopez, J.; van Aalten, D. M.; Hurtado-Guerrero, R.; Rovira, C. A Trapped Covalent Intermediate of a Glycoside Hydrolase on the Pathway to Trans-glycosylation. Insights from Experiments and Quantum Mechanics/Molecular Mechanics Simulations. *J. Am. Chem. Soc.* **2016**, *138*, 3325−3332.
(49) Zechel, D. L.; Withers, S. G. Glycosidase mechanisms: Anatomy of a finely tuned catalyst. *Acc. Chem. Res.* **2000**, *33*, 11−18.
(50) Hine, J. The Principle of Least Nuclear Motion. *Adv. Phys. Org. Chem.* **1977**, *15*, 1−61.
(51) Sinnott, M. L. The Principle of Least Nuclear Motion and the Theory of Stereoelectronic Control. *Adv. Phys. Org. Chem.* **1988**, *24*, 113−204.
(52) Silverstein, T. P. How enzymes harness highly unfavorable proton transfer reactions. *Protein Sci.* **2021**, *30*, 735−744.
(53) Kumar, P.; Agarwal, P. K.; Cuneo, M. J. On the Case of the Misplaced Hydrogens. *ChemBioChem.* **2021**, *22*, 288−297.
(54) Borshchevskiy, V.; Kovalev, K.; Round, E.; Efremov, R.; Astashkin, R.; Bourenkov, G.; Bratanov, D.; Balandin, T.; Chizhov, I.; Baeken, C.; Gushchin, I.; Kuzmin, A.; Alekseev, A.; Rogachev, A.; Willbold, D.; Engelhard, M.; Bamberg, E.; Büldt, G.; Gordeliy, V. True-atomic-resolution insights into the structure and functional role of linear chains and low-barrier hydrogen bonds in proteins. *Nat. Struct. Mol. Biol.* **2022**, *29*, 440−450.